الجمهورية الجزائرية الديمقراطية الشعبية
People's Democratic Republic of Algeria
وزارة التعليم العالي و البحث العلمي
Ministry of Higher Education and Scientific Research
جامعة عبد الحميد ابن باديس – مستغانم
Abdelhamid Ibn Badis University of Mostaganem
كلية العلوم و التكنولوجيا
Faculty of Sciences and Technology
قسم الهندسة الميكانيكية
Department of Mechanical Engineering

Order n°: M...../GM/2020

END OF CYCLE THESIS
MASTER'S DEGREE

Branch: Mechanical Engineering
Field: Energetics

Thesis

Study Of Heat Transfer In A Photovoltaic Panel By The Finite Difference Method

Presented by:

- LAIDI Radhouane Abderrahim
- LARBAOUI Abderrahmane

Presented on 30/ 06 / 2020 before the jury board composed of :

President	Dr. Bendida MEDJAHED	University of Mostaganem UMAB
Examiner	Dr. Abdelkader GUERMAT	University of Mostaganem UMAB
Supervisor	Dr. Abdelmadjid FLITTI	University of Mostaganem UMAB

Academic year: 2019 / 2020

ABSTRACT

Among the factors that decrease the efficiency of photovoltaic panels are the high operating temperatures of the PV cells. In this study, in order to predict the daily variation of these operating temperatures depending on climatic conditions, we implemented a numerical thermal model using MATLAB.

This numerical model is a transient 2D model. It is obtained by discretizing the transversal plane of the solar panel by the implicit scheme of the finite difference method.

The program developed during the study allows, not only to know the temperature distribution across the studied domain, but also to calculate some heat transfer parameters such as the total absorbed radiation, the heat exchange coefficients and the internal heat generated.

Keywords: solar panel, PV cell, finite difference method, implicit scheme and temperature.

RESUME

Parmi les facteurs qui diminuent les rendements des panneaux photovoltaïques figurent les températures de fonctionnement élevées des cellules PV. Dans cette étude, afin de prédire la variation journalière de ces températures de fonctionnement en fonction des conditions climatiques, nous avons implanté un modèle thermique numérique sous l'environnement MATLAB.

Ce modèle numérique est un modèle 2D instationnaire. Il est obtenu par la discrétisation du plan transversal du panneau solaire par le schéma implicite de la méthode des différences finies.

Le programme élaboré au cours de cette étude permet, non seulement de connaitre la distribution de la température à travers le domaine étudié, mais, également, de calculer certains paramètres de transfert thermique tels que le rayonnement total absorbé, les coefficients d'échange de chaleur et la chaleur interne générée.

Mots-clés : panneau solaire, cellule PV, méthode de différence finies, schéma implicite et température.

ملخص

تعتبر درجات حرارة التشغيل العالية للخلايا الكهروضوئية من بين أهم العوامل التي تقلل من كفاءة الألواح الشمسية. في هذه الدراسة، من أجل التنبؤ بالتغير اليومي لدرجات حرارة هذه الخلايا بدلالة الظروف المناخية، قمنا ببرمجة نموذج حراري رقمي في بيئة برنامج ماتلاب.

هذا النموذج العددي هو نموذج غير مستقر ثنائي الأبعاد. يتم الحصول عليه عن طريق تقسيم المقطع العرضي للوحة الشمسية من خلال المخطط الضمني لطريقة الفروق المنتهية.

البرنامج الذي طورناه أثناء الدراسة، لا يسمح فقط بمعرفة توزيع درجة الحرارة عبر المجال المدروس، ولكن أيضًا حساب بعض معاملات النقل الحراري مثل: إجمالي الإشعاع الممتص، معاملات التبادل الحراري والحرارة الداخلية المتولدة.

الكلمات المفتاحية: الألواح الشمسية و الخلايا الكهروضوئية و طريقة الفروق المنتهية و المخطط الضمني ودرجة الحرارة.

ACKNOWLEDGEMENT

بسم الله الرحمن الرحيم

الحمد لله على فضله و إحسانه و الشكر له على توفيقه، أما بعد ..

This work would not have been possible without contributions from others.

First, we would like to thank our advisor, **Mr. Abdelmadjid FLITTI**, for his continued patience.

whenever we had any academic problems with this thesis. We determined our career goals after taking so many courses such as numerical methods taught by himself. We would also like to sincerely thank him for taking an interest in and offering advice about our life outside of academia.

We express our gratitude to **Mr. Bendida MEDJAHED**, for having done us the honour of presiding over the jury of our memory and to **Mr. Abdelkader GUERMAT** for accepting to examine our work.

We are also grateful to the rest of the professors who helped forming us through our universal journey,

Finally, we would like to thank our families and friends for

their continued support during our educational course.

DEDICATIONS

To the people dearest to my heart,

My mom and my dad, may God bless them and keep them in good health,

my younger brother, and my lovely sister Amel who has been there for me and guided me through every step in my way to success...

To all my friends and family ...

I dedicate this modest work...

Radhouane Abderrahim

This work is wholeheartedly dedicated to my beloved parents, who have been my source of inspiration and gave me strength when I thought of giving up, continually provide their moral, spiritual, emotional, and financial support.

To my brothers, relatives, friends and classmates who shared their words of advice and encouragement to finish this study.

Abderrahmane

TABLE OF CONTENTS

LIST OF FIGURES

LIST OF TABLES

NOMENCLATURE

A: the area (m^2).
c: the specific heat capacity of material (J/Kg °K).
e: the thickness of material (m).
G_{POA}: the measured incident POA irradiance (W/m^2).
Gr: the Grashof number (dimensionless).
h_{con} : the convection exchange coefficient (W/ m^2. °K).
h_{rad} : the coefficient of exchange by radiation sky (W/ m^2. °K).
k: coefficient of thermal conductivity of the material (W/ m. °K).
L: the characteristic length (m).
Nu: the Nusselt number (dimensionless).
Pr: the Prandtl number (dimensionless).
Q: the generated heat (W).
q_{con}: connective heat flow (W).
q_{rad}: radiant heat flow (W).
Ra: the Rayleigh number (dimensionless).
Re: the Reynolds number (dimensionless).
S: the measured solar radiation falling on the tilted PV panel (W/ m^2).
T: the temperature (°C).
t : the time (s).
V : the volume (m^3).
ws: the wind speed (m/s).

Greek symbols

$\tilde{\alpha}$: is the effective absorption (dimensionless).
β: is the tilt angle of the panel in regard to the horizontal plane (degrees°).
γ: is the surface azimuth angle (degrees°).
θ_z: is the Zenith angle (degrees°).
θ_b: is the angle of incidence of the beam irradiation (degrees°).
θ_r : is the refracted angle through the front glass glazing layer (degrees°).
γ_s: is the solar azimuth angle (degrees°).
η: the efficiency.
δ: is the declination (degrees°).
ω: is the hour angle (degrees°).
$\mathcal{E}$: is the emissivity (dimensionless).
Φ: the heat flow (W).
ρ: density of the material (Kg/m^3).
ν: is the the kinematic viscosity of air (m^2/s).
μ: is the dynamic viscosity of air (kg/m.s).
σ: is the Stefan-Boltzmann constant. (w/m°K).

Subscripts

air: air.
amb: ambient.
$cell$: photovoltaic cells
$conv$: convective.
e: entering.
fg: front glass.
$film$: film.
g: generated.
gr: ground.
PV: photovoltaic.
rad: radiative.
Sky: sky.
st: stored.
sur: surface.

INTRODUCTION

The geographical position of Algeria provides it with one of the most important solar deposits in the world. Indeed, the average national annual insolation time exceeds 2000 hours [Gov 20] and a horizontal surface of 1m² receives an annual energy of nearly 3 KWh/m² in the north and more than 5.6 KWh/m in the south [Gov 20]. In order to exploit this resource, Algeria has set up a national programme, which is spread over fifteen years, to produce, by 2030, 13575 MW of electricity from photovoltaic energy [Era 20].

Solar panels convert solar radiation into electricity using photovoltaic cells. The efficiency of most of them varies between 13 and 20% [Irwanto 14]. As a result, most of the energy received by the cell accumulates as heat, which then causes a considerable increase in the temperature of the PV cells [Dubey 13]. This increase, against all expectations, reduces the efficiency of the PV panel Dubey 13]. In this context, this work consists of developing a program to study the temperature variation of PV cells under the effect of daily weather conditions. The literature proposes several thermal models [Aly 18, Aly2 17, Siddiqui 12, Zondag 02], but our choice was made for the 2D model proposed by Aly et al [Aly2 17]. This model is obtained using the implicit scheme of the finite difference method. In order to test the developed program, we consider the estimated meteorological data.

To carry out this study, our thesis is organized in three chapters:

- The first chapter covers generalities about solar panels;
- The second chapter describes in detail the methodology for obtaining the thermal model;
- The third chapter presents and discusses the results obtained.

Chapter I : Generalities on Photovoltaic panels

I.1. Historical overview

The photovoltaic effect or the PV effect was discovered in the early 19th century. In 1839, a young French physicist “Alexandre Edmond Becquerel” observed a physical phenomenon that allows the conversion of light into electricity, that’s the principle of photovoltaic effect, which is used in solar cells [Čotar 12]. In the years that followed, a number of scientists have contributed in the development of this effect and technologies through their research, the most relevant among them are Charles Fritts, Edward Weston, Nikola Tesla and Albert Einstein who has been awarded the Nobel Prize for his work on "photoelectric effect" on 1904. However, due to high production rates, greater development of the technology hasn’t been made until the rise of semiconductor industry by the late fifties of the 20th century [Čotar 12].

During the sixties, solar cells were used exclusively for supplying orbiting satellites, where they proved to be a cheap reliable technology. In the seventies there has been improvements in production while the oil crisis helped reduce the cost of solar cells and opened up new possibilities for their implementation. Solar cells were immediately recognized as an obvious alternative for electricity supply in locations isolated from the power grid, the harvested energy was used in wireless applications, lighthouses' batteries, telecommunication equipment and other low power electricity dependent equipment. During the eighties, solar cells have become popular as an energy source for consumer electronic devices including calculators, watches, radios, lamps and other applications with small batteries. Also, after the crisis in the seventies, great efforts were made in the development of solar cells for commercial use in households. Independent solar cells systems (off-grid) have been developed, as well as network connected systems (on-grid). Meanwhile, a significant increase in use of solar cells has been recorded in rural areas where the power network and infrastructure are under-

developed. Photovoltaic modules technology and market development has grown rapidly by introducing incentives to produce electricity from renewable energy sources [Čotar 12].

Figure I.1: PV panels [Energy 20].

I.2. PV Technology

Unlike other renewable energy sources, PV technology has an advantage of being easily accessible and employed, both at small and large scales. One needs to entirely model the PV system to accurately predict the overall performance under customized service conditions. A robust PV system model is a multi-physics model that usually consists of radiation model, thermal model, electrical model and in some cases, structural model.

What defines a PV model is its power output. It demands certain parametric inputs such as the temperature of the PV cell under operation, which can be calculated using a thermal model.

A photovoltaic system is made up of several photovoltaic solar cells. Each PV cell can generate about 1 or 2 Watts of power depending on the materials of its components. For higher power output, multiple PV cells can be combined to produce higher power modules which are limited at 1 Kw in the market but can be increased at need [Sumathi 15].

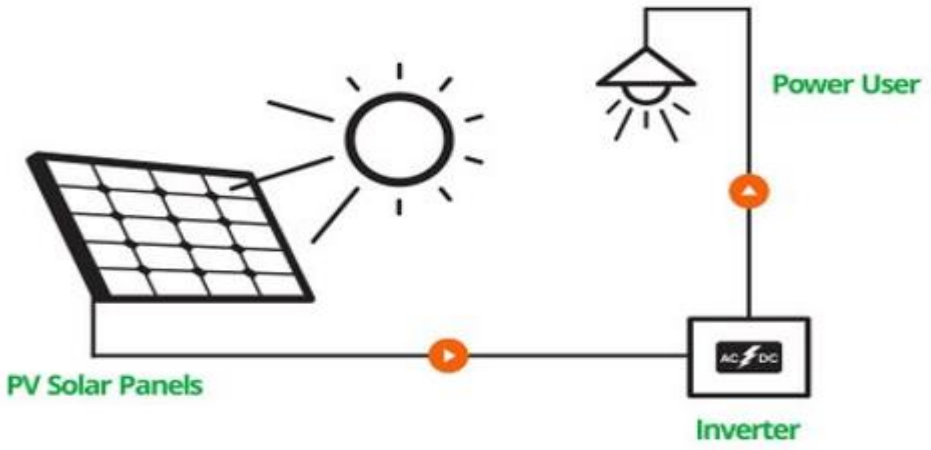

Figure I.2: A simple PV system [India 20].

I.3. PV cells

The solar cell is the elementary building block and the most important component of the photovoltaic technology. Solar cells are made of semiconductor materials such as silicon. One of the properties of semiconductors that make them most useful is their conductivity, which may easily be modified by introducing impurities into their crystal lattice.

Figure I. 3: A Photovoltaic cell [Alive 20].

I.4. Functioning of the photovoltaic cells

The most known use of solar energy is converting it into electricity in a photovoltaic installation using solar cells**.**

Power conversion through a solar cell follows a simple physical phenomenon, photons strike and ionize semiconductor material on the solar panel, causing outer electrons to break free of their atomic bonds. Due to the semiconductor structure, the electrons are forced in one direction creating a flow of electrical current. Solar cells are not 100% efficient in crystalline silicon solar cells, in part because only a portion of the light within the spectrum can be absorbed. Some of the light spectrum is reflected, some is too weak to create electricity (infrared) and some (ultraviolet) creates heat energy instead of electricity (shown in Fig I.4) [Seia 20]**.**

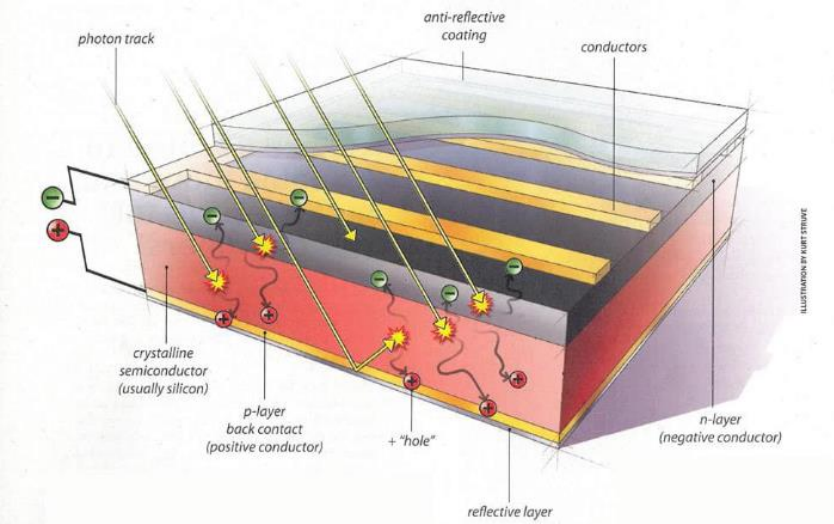

Figure I.4: Functioning of a photovoltaic cell [Seia 20].

I.5. PV panels different types

I.5.1. Monocrystalline Solar Panels

Monocrystalline panels are the most efficient type of solar panels, but they can be very sensitive and have a low tolerance to shading and dirt, even the shading of one solar can cause a 20% draw-back in performance. They can get very expensive too [Solarp 20].

Figure I. 5: Monocrystalline Solar Panel[Solarm 20].

I.5.2. Polycrystalline Solar Panels

Polycrystalline panels are slightly less efficient but cost 30-50% less than monocrystalline ones when intended to produce the same amount of power.

Theoretically, polycrystalline panels have a lifespan of about 25 years, In the field though they proved to be perfectly operational for even longer [Solarp 20].

Figure I. 6: Polycrystalline panel [Solarm 20].

I.5.3. Thin-film panels

Thin-film panels are the cheapest panels with the lowest efficiency – usually half the efficiency of monocrystalline panels. Therefore, to generate the same amount of power we need twice the number of thin-film panel.

Figure I.7: A Thin-film panel [Clean 20].

I.6. PV panels efficiency

The measure of how well solar panels absorb sunlight and convert it to electrical energy is called *efficiency*. Light travels in different wavelengths of varying energy levels across the bands of the electromagnetic spectrum, and not all is absorbed by a solar panel. Measured in electron volts (eV), the typical band gap energy which can be absorbed and transformed by a solar panel into electricity is about 1.1 eV [Solarm 20].

In recent years, extensive research is focusing on improving the efficiency of solar cells for commercial use. Monocrystalline silicon solar cells have been showing constant improvements year by year. It started with only 15% in 1950s and then increased to 17% in 1970s and up to 28% nowadays. According to Zhao et al [Zhao 99].

In the table below we may find approximated values of different efficiencies of different types of PV cells:

Table I. 1: PV cell's efficiencies [Spirit 20]

Type of Cell	**Panel Efficiency**
Monocrystalline	16% - 20%
Polycrystalline	15% - 17%
Thin Film	12% -14%

I.7. Advantages and drawbacks of PV solar energy

The main advantages of photovoltaic panels are [Zeman 10]:

- environmentally friendly, with no emissions nor harmful waste;
- noiseless due to not having any moving parts ;
- long lifespan, up to 30 years with minimal maintenance requirements;
- power can be generated from any light source, solar or artificial;
- PV operates even in cloudy weather conditions;
- modular or “custom-made” energy, can be designed for any application from watch to a multi-megawatt power plant.

However, they have the following disadvantages [Zeman 10]:

- high initial costs that overshadow the low maintenance and lack of fuel costs;
- large area needed for large scale applications;
- PV generates direct current: special DC appliances or inverters are needed;
- off-grid applications require energy storage, such as batteries.

Chapter II: Thermal transfer modelling in the "ND-220E1F" panel by the finite difference method

II.1. Introduction

The finite difference method (FDM) is one of the most frequently used numerical methods for solving partial differential equations [Necati 17]. It is based on the approximation of the partial derivatives of a function, at a point, by combining the point values of this function into a finite number of neighbouring points in space or time [Azzi 11, Silva 07]. Thus, the solution of the partial differential equation is substituted by the search for the solution of a linear system [Giovannini 12].

The main advantage of this method lies in the great simplicity of writing and the low cost of calculation. [Silva 07]. However, it has the following limitations: it is only suitable for simple geometries and it is difficult to take Neumann boundary conditions into account [Silva 07].

II.2. Implicit scheme for solving the unsteady 2D heat equation

The temperature field T (x, y) in a two-dimensional domain D is given by the following partial differential equation:

$$\frac{\partial}{\partial x}\left(k_x \frac{\partial T}{\partial x}\right) + \frac{\partial}{\partial y}\left(k_y \frac{\partial T}{\partial y}\right) + Q = \rho c \frac{\partial T}{\partial t} \quad \textbf{(II.1)}$$

Where:

- k_x**:** coefficient of thermal conductivity of the material in the ***ox*** direction;
- k_y**:** coefficient of thermal conductivity of the material in the ***oy*** direction;
- Q**:** generated heat;
- ρ**:** density of the material;
- **c:** heat mass capacity of the material.

If k_x and k_y are constants, the relation (II.1) takes the following form:

$$k_x \frac{\partial^2 T}{\partial x^2} + k_y \frac{\partial^2 T}{\partial y^2} + Q = \rho c \frac{\partial T}{\partial t} \quad \textbf{(II.2)}$$

The studied field is discretized in space and time. By dividing space into segments Δx and Δy following the coordinates x and y respectively [Benbrik 18, Silva 07]. Time is discretized in constant step intervals Δt . Thus, the nodes' identification is achieved as follows [Benbrik 18, Silva 07]:

- the index i locates the abscissa of the node ($x_i = i\,\Delta x$) ;
- the index j locates the ordinate of the node ($y_j = j\,\Delta y$) ;
- the index p locates time ($t_p = p\,\Delta t$).

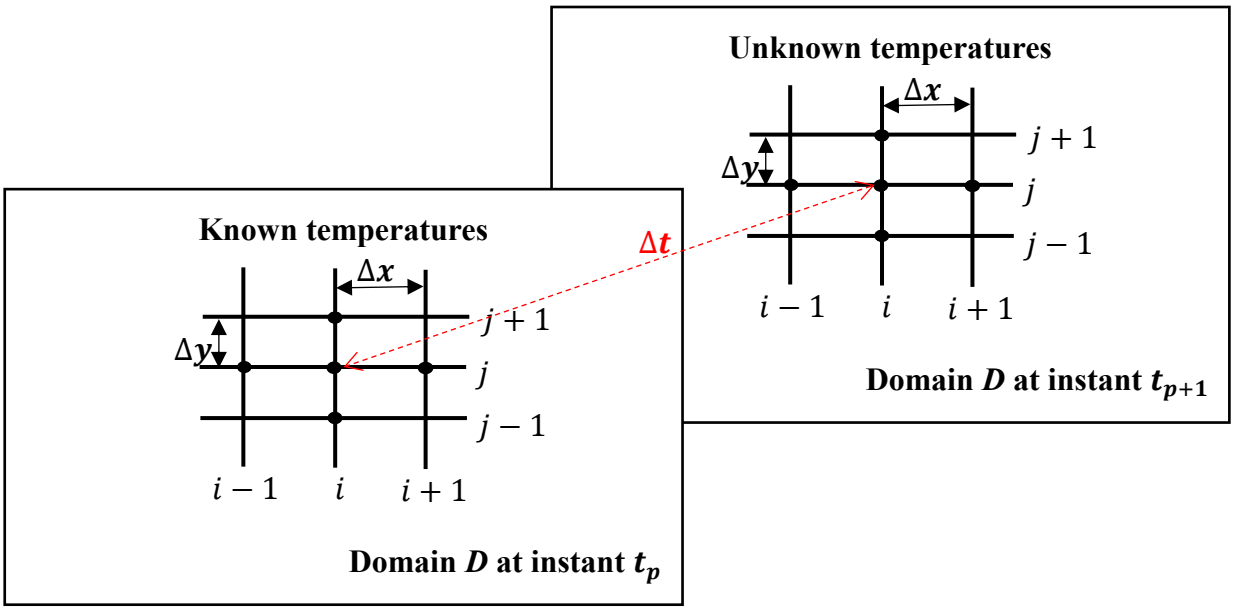

Figure II.1: Molecular representation of the implicit scheme.

For the implicit scheme, equation (III.2) is discretized at (x_i, y_j) at instant t_{p+1} and the evaluation [Necati 17]:

- of the second derivatives in space of the function $T(x, y, t)$ is done using a second order central differencing scheme;
- of the first derivative in time is realized using a first-order backward scheme.

Using the following notation: $T_{i,j}^{p}$, which represents the discrete temperature $T(x_i, y_j, t_p)$ at node (x_i, y_j) at the instant t_p, the derivatives expressed in the formula (II.2) , are defined according to the implicit scheme as follows [Necati 17]:

$$\frac{\partial^2}{\partial x^2} T(x_i, y_j, t_{p+1}) = \frac{T_{i-1,j}^{p+1} - 2\,T_{i,j}^{p+1} + T_{i+1,j}^{p+1}}{\Delta x^2} \qquad \textbf{(II.3)}$$

$$\frac{\partial^2}{\partial y^2} T(x_i, y_j, t_{p+1}) = \frac{T_{i,j-1}^{p+1} - 2\,T_{i,j}^{p+1} + T_{i,j+1}^{p+1}}{\Delta y^2} \qquad \textbf{(II.4)}$$

$$\frac{\partial}{\partial t} T(x_i, y_j, t_{p+1}) = \frac{T_{i,j}^{p+1} - T_{i,j}^{p}}{\Delta t} \qquad \textbf{(II.5)}$$

Thus, the discrete form of the equation (III.2) for interior points is as follows:

$$\left(1+\frac{2\Delta t}{\rho c}\left(\frac{k_x}{\Delta x^2}+\frac{k_y}{\Delta y^2}\right)\right)T_{i,j}^{p+1}-\left(\frac{\Delta t}{\rho c}\frac{k_x}{\Delta x^2}\right)T_{i-1,j}^{p+1}-\left(\frac{\Delta t}{\rho c}\frac{k_x}{\Delta x^2}\right)T_{i+1,j}^{p+1}-\left(\frac{\Delta t}{\rho c}\frac{k_y}{\Delta y^2}\right)T_{i,j-1}^{p+1}-\left(\frac{\Delta t}{\rho c}\frac{k_y}{\Delta y^2}\right)T_{i,j+1}^{p+1}=T_{i,j}^{p}+\frac{\Delta t}{\rho c}Q_{i,j} \quad \textbf{(II.6)}$$

This equation can be determined, using the control volume method, as follows [Aly 17, Benbrik 18 et Çengel 03], from the energy balance.

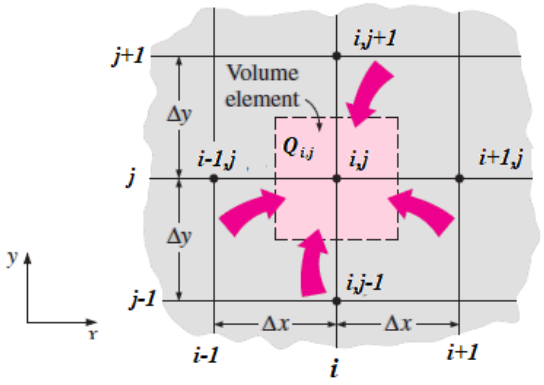

Figure II.2: Energy balance of the control volume [Çengel 03].

Considering the example of the internal node shown in figure II.2, the thermal energy balance is given by [Aly2 17, Benbrik 18 and Çengel 03]:

$$\Phi_e+\Phi_g=\Phi_{st} \quad \textbf{(II.7)}$$

where:

- Φ_e: the entering heat flow;
- Φ_g: the generated heat flow;
- Φ_{st}: the stored heat flow.

The three heat flows are given by the following formulas [Aly2 17, Çengel 03]:

$$\Phi_e=\Delta y\,k_x\frac{T_{i-1,j}^{p+1}-T_{i,j}^{p+1}}{\Delta x}+\Delta y\,k_x\frac{T_{i+1,j}^{p+1}-T_{i,j}^{p+1}}{\Delta x}+\Delta x\,k_y\frac{T_{i,j-1}^{p+1}-T_{i,j}^{p+1}}{\Delta y}+\Delta x\,k_y\frac{T_{i,j+1}^{p+1}-T_{i,j}^{p+1}}{\Delta y} \quad \textbf{(II.8)}$$

$$\Phi_g=\Delta x\Delta y\,Q_{i,j} \quad \textbf{(II.9)}$$

$$\Phi_{st}=\Delta x\Delta y\,\rho\,c\frac{T_{i,j}^{p+1}-T_{i,j}^{p}}{\Delta t} \quad \textbf{(II.10)}$$

By inputting these last three equations into formula II.7 and dividing by $(\Delta x\Delta y)$, we get the following formula:

$$k_x\frac{T_{i-1,j}^{p+1}-2\,T_{i,j}^{p+1}+T_{i+1,j}^{p+1}}{\Delta x^2}+k_y\frac{T_{i,j-1}^{p+1}-2\,T_{i,j}^{p+1}+T_{i,j+1}^{p+1}}{\Delta y^2}+Q_{i,j}=\rho\,c\frac{T_{i,j}^{p+1}-T_{i,j}^{p}}{\Delta t} \quad \textbf{(II.11)}$$

When rearranging this equation, we get equation II.6.

II.3. Composition of the photovoltaic panel under study

The photovoltaic panel studied in this work is a Sharp polycrystalline "ND-220E1F" panel. It is 1652 mm long and 994 mm wide. It consists mainly of the following layers [Aly1 17, Aly2 17]:

- **A glass layer:** 3 mm thick, forming the front surface;
- **Two layers of ethylene vinyl acetate (EVA)**: each layer is 0.15 mm thick and protects the photovoltaic cell. The low cost of EVA and its favourable physical properties (good weather resistance, high optical transparency and ease of processing) make it an ideal encapsulation material [Banaceur 19];

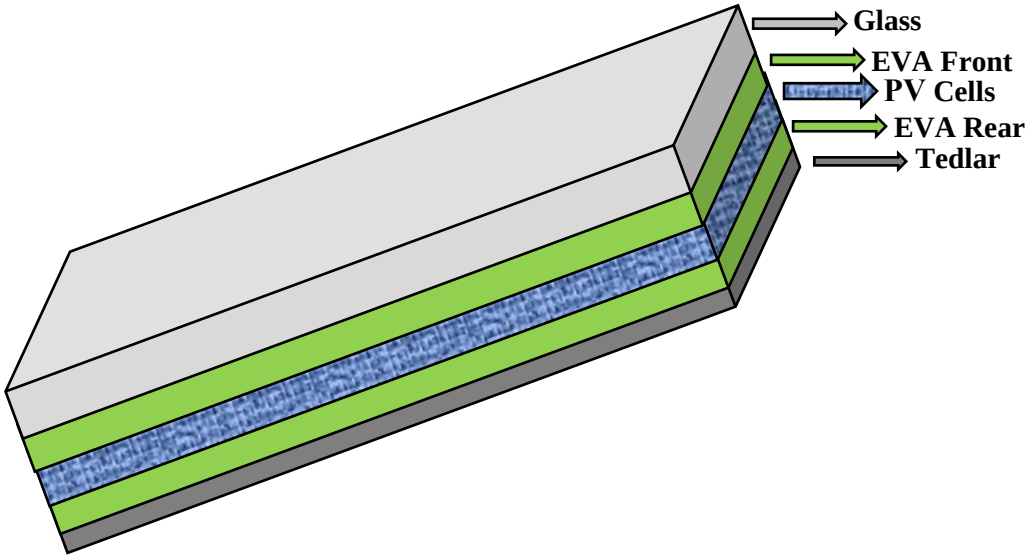

Figure II. 3: Main layers of the photovoltaic panel.

- **Photovoltaic cells:** is the site of electric power generation. The ND-220E1F panel contains 60 photovoltaic cells each is 156.5 × 156.5 mm in size;
- **Tedlar layer:** Tedlar is a polyvinyl fluoride film [Banaceur 19].

It should be noted that thin layers, such as the anti-reflective coating (ARC) layer, are not considered in this work. The physical properties of the various layers are shown in the table II.1 below:

Table II.1: Physical properties of the different layers [Aly2 17, Armstrong 10].

Layer	e (mm)	$k\ (w/m\ K)$	$\rho\ (kg/m^3)$	$c\ (J/kg\ K)$
Glass	3	1.8	3000	500
EVA Front	0.15	0.35	960	2090
PV Cell	0.225	148	2330	677
EVA Rear	0.15	0.35	960	2090
Tedlar	0.1	0.2	1200	1250

II.4. Thermal model

The geometric model of this study is a two-dimensional model that represents a cross-section of the solar panel (see figure II.4). The heat exchange is symmetrical to the axis in the middle of the crosscut. Thus, only the left half is studied.

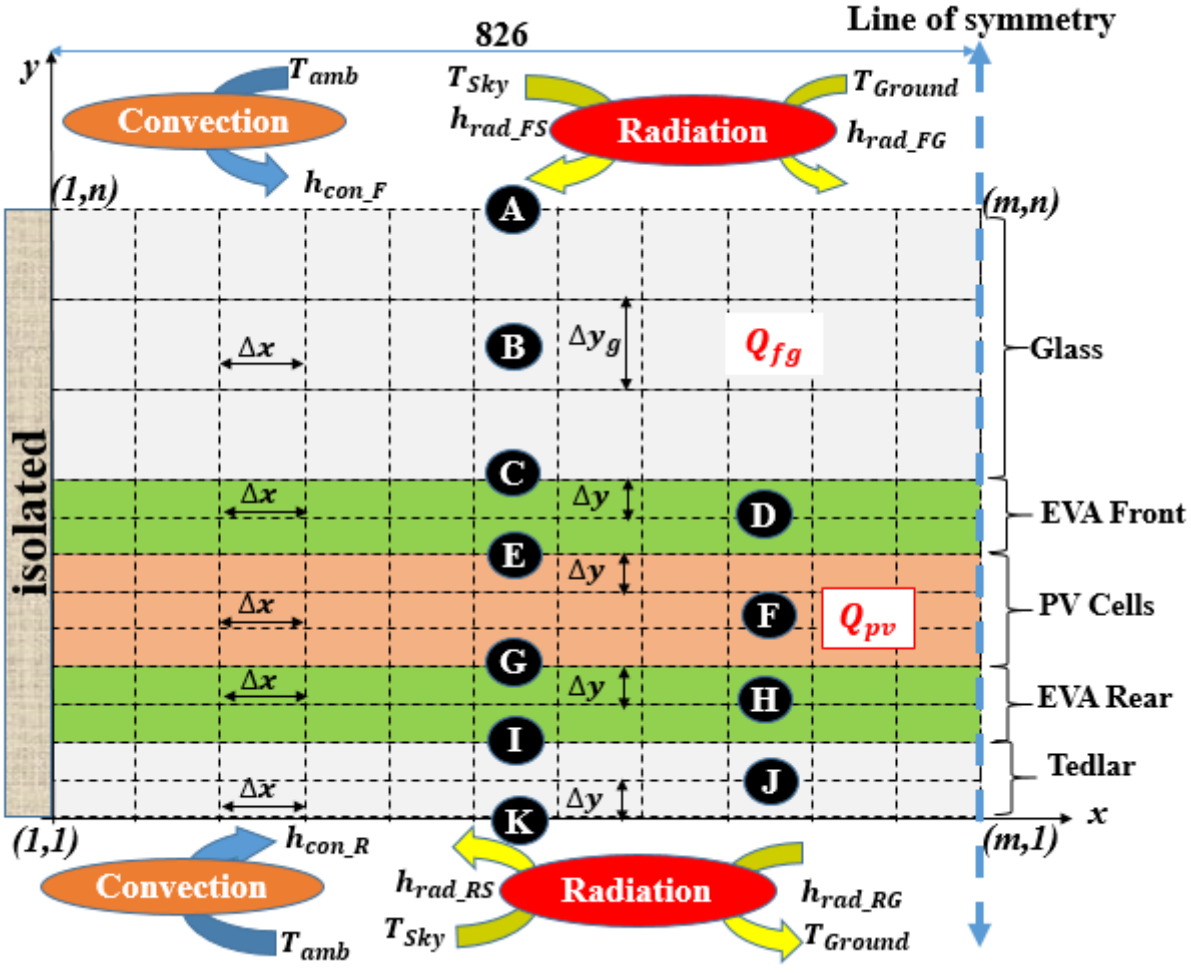

Figure II. 4: 2D grid of half the photovoltaic panel (figure not to scale) with boundary conditions [Aly2 17, Aly 18].

II.4.1. Discretization of the field of study

Solving the heat equation by the finite difference method requires discretizing the domain under study to form the computing grid. For our model, the spatial step Δx **,** depending on the direction ***x,*** is identical for all PV layers. While for direction ***y*** two steps were chosen: Δy_g for the glass layer and Δy for the other layers (see figure II.4). The grid has ***N*** nodes (***m********n***). After discretization, the resulting nodes can be categorized from one of the following families (see figure II.4):

- **Surface nodes:** nodes of types '**A**' and '**K**' and within the domain boundaries, except for the four corners;
- **Internal nodes:** nodes of types 'B', 'D', 'F', 'H' et 'J';
- **Interface nodes:** nodes of types 'C', 'E', 'G' et 'I' ;
- **Outer corner nodes:** all around the four corners of the domain.

II.4.2. Boundary conditions and assumptions

The borderline conditions at the boundaries of the photovoltaic panel, assumed in the current study, are the following:

- **Upper side of the glass layer and lower side of the Tedlar layer:** each side exchanges heat by convection with the outside and by radiation with the environment. The linearized forms of these modes of transfer are expressed as follows [Aly1 17, Aly 18]:

$$q_{con\_F/con\_R} = h_{con\_F/con\_R}\,(T_{Sur} - T_{amb}) \quad \textbf{(II.12)}$$

$$q_{rad\_F/rad\_R} = h_{rad\_FS/rad\_RS}\,(T_{Sur} - T_{Sky}) + h_{rad\_FG/rad\_RG}\,(T_{Sur} - T_{Gr}) \quad \textbf{(II.13)}$$

Where:

q_{con_F/con_R}: connective heat flow glass side/Tedlar side;

h_{con_F/con_R}: convection exchange coefficient glass side / Tedlar side;

T_{sur}: wall temperature;

T_{amb}: ambient temperature;

q_{rad_F/rad_R}: radiant heat flow glass side/Tedlar side;

h_{rad_FS/rad_RS}: coefficient of exchange by radiation glass_sky/ Tedlar_sky;

T_{Sky}: the sky temperature;

h_{rad_FG/rad_RG}: coefficient of exchange by radiation glass-ground/ Tedlar-ground;

T_{Gr}: the ground Temperature.

- **Left side:** the left side is assumed to be heat-insulated.

Only the glass and photovoltaic cell layers are assumed to be capable of generating heat.

II.4.3. Formulating the equations

II.4.3.1. Internal Nodes

The finite difference formulation of the internal nodes is directly derived from the equation (II.6):

$$\mathbf{L_1}\left(\left(\frac{1}{\mathbf{L_1}}+2\,k_{mat}\left(\frac{\Delta y_c}{\Delta x}+\frac{\Delta x}{\Delta y_c}\right)\right)T_{i,j}^{p+1}-\frac{\Delta y_c}{\Delta x}\,k_{mat}\left(T_{i-1,j}^{p+1}+T_{i+1,j}^{p+1}\right)-\,k_{mat}\,\frac{\Delta x}{\Delta y_c}\left(T_{i,j-1}^{p+1}+T_{i,j+1}^{p+1}\right)\right)$$
$$=T_{i,j}^{p}+\,\mathbf{L_1}\Delta x\,\Delta y_c\,Q_c \qquad \textbf{(II.14)}$$

with:

$$\mathbf{L_1}=\frac{\Delta t}{\rho_{mat}\,c_{mat}\,\Delta x\,\Delta y_c}$$

In the equation above:

- The index ***mat*** denotes the material of the layer where the node is located;
- Δy_c is equal to Δy_g for the glass layer and to Δy for the other layers;
- $Q_c = Q_{fg/pv}$ for the (glass / PV cell) layer, and it is equal to zero for the others.

II.4.3.2. Type A nodes

They are the nodes on the upper side of the solar panel. (***j=n***).

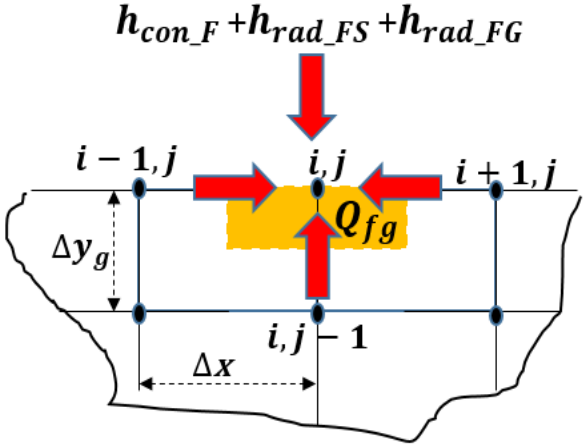

Figure II.5: Balance of a type A nodes.

The heat energy balance at the node of II.5 provides the following equation:

$$\frac{\Delta y_g}{2}\, k_g\, \frac{T_{i-1,j}^{p+1}-T_{i,j}^{p+1}}{\Delta x}+\frac{\Delta y_g}{2}\, k_g\, \frac{T_{i+1,j}^{p+1}-T_{i,j}^{p+1}}{\Delta x}+\Delta x\, k_g\, \frac{T_{i,j-1}^{p+1}-T_{i,j}^{p+1}}{\Delta y_g}+\Delta x\, h_{con\_F}\left(T_{amb}^{p+1}-T_{i,j}^{p+1}\right)+$$

$$\Delta x\, h_{rad\_FS}\left(T_{Sky}^{p+1}-T_{i,j}^{p+1}\right)+\Delta x\, h_{rad\_FG}\left(T_{Gr}^{p+1}-T_{i,j}^{p+1}\right)+\Delta x\frac{\Delta y_g}{2}\, Q_{fg}=\Delta x\, \frac{\Delta y_g}{2}\, \rho_g\, c_g\, \frac{T_{i,j}^{p+1}-T_{i,j}^{p}}{\Delta t} \quad \textbf{(II.15)}$$

After transformation, we get the following expression:

$$\mathrm{L}_2\left(\left(\frac{1}{\mathrm{L}_2}+\frac{\Delta y_g}{\Delta x}\, k_g+\frac{\Delta x}{\Delta y_g}\, k_g+\Delta x\,(h_{con\_F}+h_{rad\_FS}+h_{rad\_FG})\right)T_{i,j}^{p+1}-\frac{\Delta y_g}{2\,\Delta x}\, k_g T_{i-1,j}^{p+1}-\frac{\Delta y_g}{2\,\Delta x}\, k_g T_{i+1,j}^{p+1}-\right.$$

$$\left. k_g\, \frac{\Delta x}{\Delta y_g} T_{i,j-1}^{p+1}\right)=T_{i,j}^{p}+\mathrm{L}_2(\Delta x\frac{\Delta y_g}{2}\, Q_{fg}+\Delta x\, \left(h_{con\_F}\, T_{amb}^{p+1}+h_{rad\_FS}\, T_{Sky}^{p+1}+h_{rad\_FG}\, T_{Gr}^{p+1}\right)) \quad \textbf{(II.16)}$$

With:

$$\mathrm{L}_2=\frac{2\Delta t}{\rho_g\, c_g\, \Delta x\, \Delta y_g}$$

Equation II.16 becomes:

- On the left corner (Node (1, n)) as follows:

$$\mathrm{L}_2\left(\left(\frac{1}{\mathrm{L}_2}+\frac{\Delta y_g}{\Delta x}\, k_g+\frac{\Delta x}{\Delta y_g}\, k_g+\Delta x\,(h_{con\_F}+h_{rad\_FS}+h_{rad\_FG})\right)T_{i,j}^{k+1}-\frac{\Delta y_g}{\Delta x}\, k_g T_{i+1,j}^{k+1}-\, k_g\, \frac{\Delta x}{\Delta y_g} T_{i,j-1}^{k+1}\right)=$$

$$T_{i,j}^{k}+\mathrm{L}_2(\Delta x\frac{\Delta y_g}{2}\, Q_{fg}+\Delta x\, \left(h_{con\_F}\, T_{amb}^{k+1}+h_{rad\_FS}\, T_{Sky}^{k+1}+h_{rad\_FG}\, T_{G}^{k+1}\right)) \quad \textbf{(II.17)}$$

- On the right corner (Node (m, n)) as follows:

$$\mathrm{L}_2\left(\left(\frac{1}{\mathrm{L}_2}+\frac{\Delta y_g}{\Delta x}\, k_g+\frac{\Delta x}{\Delta y_g}\, k_g+\Delta x\,(h_{con\_F}+h_{rad\_FS}+h_{rad\_FG})\right)T_{i,j}^{p+1}-\frac{\Delta y_g}{\Delta x}\, k_g T_{i-1,j}^{p+1}-\, k_g\, \frac{\Delta x}{\Delta y_g} T_{i,j-1}^{p+1}\right)=$$

$$T_{i,j}^{p}+\mathrm{L}_2(\Delta x\frac{\Delta y_g}{2}\, Q_{fg}+\Delta x\, \left(h_{con\_F}\, T_{amb}^{p+1}+h_{rad\_FS}\, T_{Sky}^{p+1}+h_{rad\_FG}\, T_{Gr}^{p+1}\right)) \quad \textbf{(II.18)}$$

II.4.3.3. Type K nodes

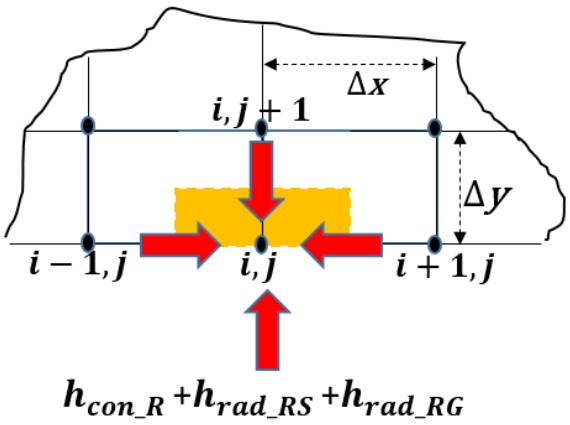

Figure II. 6: Balance of a type K nodes.

From the previous section, we can conclude that the energy balance of a type K node leads to the following result:

$$\mathbf{L_3}\left(\left(\frac{1}{\mathbf{L_2}}+\frac{\Delta y}{\Delta x}\,\boldsymbol{k_t}+\frac{\Delta x}{\Delta y}\,\boldsymbol{k_t}+\Delta x\,(\boldsymbol{h_{con\_F}}+\boldsymbol{h_{rad\_FS}}+\boldsymbol{h_{rad\_FG}})\right)\boldsymbol{T_{i,j}^{p+1}}-\frac{\Delta y}{2\,\Delta x}\,\boldsymbol{k_t}\boldsymbol{T_{i-1,j}^{p+1}}-\frac{\Delta y}{2\,\Delta x}\,\boldsymbol{k_t}\boldsymbol{T_{i+1,j}^{p+1}}-\boldsymbol{k_t}\,\frac{\Delta x}{\Delta y}\boldsymbol{T_{i,j+1}^{p+1}}\right)=\boldsymbol{T_{i,j}^{p}}+\mathbf{L_3}(\Delta x\,\left(\boldsymbol{h_{con\_R}}\,\boldsymbol{T_{amb}^{p+1}}+\boldsymbol{h_{rad\_RS}}\,\boldsymbol{T_{Sky}^{p+1}}+\boldsymbol{h_{rad\_RG}}\,\boldsymbol{T_{Gr}^{p+1}}\right)) \qquad \textbf{(II.19)}$$

With:

$$\mathbf{L_3}=\frac{2\Delta t}{\boldsymbol{\rho_t}\,\boldsymbol{c_t}\,\Delta x\,\Delta y}$$

II.4.3.4. Type C nodes

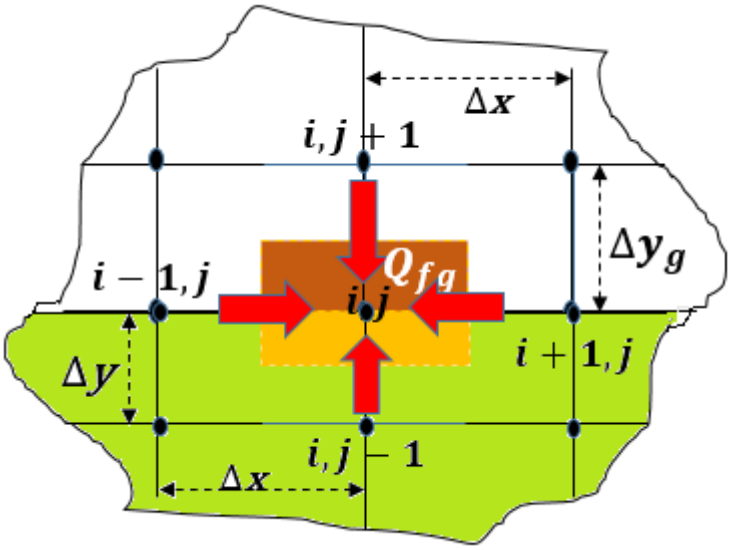

Figure II. 7: Balance of a type C nodes.

Type C nodes are located at the glass-EVA interface; based on figure II.7 the energy balance of these nodes leads to the following relation:

$$\left(\frac{\Delta y_g}{2}\,\boldsymbol{k_g}+\frac{\Delta y}{2}\,\boldsymbol{k_e}\right)\frac{\boldsymbol{T_{i-1,j}^{p+1}}-\boldsymbol{T_{i,j}^{p+1}}}{\Delta x}+\left(\frac{\Delta y_g}{2}\,\boldsymbol{k_g}+\frac{\Delta y}{2}\,\boldsymbol{k_e}\right)\frac{\boldsymbol{T_{i+1,j}^{p+1}}-\boldsymbol{T_{i,j}^{p+1}}}{\Delta x}+\Delta x\,\boldsymbol{k_e}\,\frac{\boldsymbol{T_{i,j-1}^{p+1}}-\boldsymbol{T_{i,j}^{p+1}}}{\Delta y}+$$

$$\Delta x\,\boldsymbol{k_g}\,\frac{\boldsymbol{T_{i,j+1}^{p+1}}-\boldsymbol{T_{i,j}^{p+1}}}{\Delta y_g}++\Delta x\,\frac{\Delta y_g}{2}\,\boldsymbol{Q_{fg}}=\frac{\Delta x}{2}\,(\Delta y_g\,\boldsymbol{\rho_g}\,\boldsymbol{c_g}+\Delta y\,\boldsymbol{\rho_e}\,\boldsymbol{c_e})\,\frac{\boldsymbol{T_{i,j}^{p+1}}-\boldsymbol{T_{i,j}^{p}}}{\Delta t} \qquad \textbf{(II.20)}$$

By arranging in the implicit form:

$$\mathbf{L_4}\left(\left(\frac{1}{\mathbf{L_4}}+\frac{k_g\,\Delta y_g+k_e\,\Delta y}{\Delta x}+\frac{\Delta x}{\Delta y}\,k_e+\frac{\Delta x}{\Delta y_g}\,k_g\right)T_{i,j}^{p+1}-\frac{k_g\,\Delta y_g+k_e\,\Delta y}{2\,\Delta x}T_{i-1,j}^{p+1}-\frac{k_g\,\Delta y_g+k_e\,\Delta y}{2\,\Delta x}T_{i+1,j}^{p+1}-\frac{\Delta x}{\Delta y}\,k_e\,T_{i,j-1}^{p+1}-\frac{\Delta x}{\Delta y_g}\,k_g\,T_{i,j+1}^{p+1}\right)=T_{i,j}^{p}+\mathbf{L_4}\left(\Delta x\,\frac{\Delta y_g}{2}\,Q_{fg}\right)\qquad\textbf{(II.21)}$$

With:

$$\mathbf{L_4}=\frac{2\Delta t}{\Delta x(\Delta y_g\,\rho_g\,c_g+\Delta y\,\rho_e\,c_e)}$$

II.4.3.5. Nodes of types E, G and I

Based on the results found in section II.4.3.4, we get the equations:

- **Type E nodes**

$$\mathbf{L_5}\left(\left(\frac{1}{\mathbf{L_5}}+\frac{(k_{pv}+k_e)\Delta y}{\Delta x}+\frac{\Delta x}{\Delta y}\,k_e+\frac{\Delta x}{\Delta y}\,k_{pv}\right)T_{i,j}^{p+1}-\frac{(k_{pv}+k_e)\Delta y}{2\,\Delta x}T_{i-1,j}^{p+1}-\frac{(k_{pv}+k_e)\Delta y}{2\,\Delta x}T_{i+1,j}^{p+1}-\frac{\Delta x}{\Delta y}\,k_{pv}\,T_{i,j-1}^{p+1}-\frac{\Delta x}{\Delta y}\,k_e\,T_{i,j+1}^{p+1}\right)=T_{i,j}^{p}+\mathbf{L_5}(\Delta x\,\frac{\Delta y}{2}\,Q_{pv})\qquad\textbf{(II.22)}$$

- **Type G nodes**

$$\mathbf{L_5}\left(\left(\frac{1}{\mathbf{L_5}}+\frac{(k_{pv}+k_e)\Delta y}{\Delta x}+\frac{\Delta x}{\Delta y}\,k_e+\frac{\Delta x}{\Delta y}\,k_{pv}\right)T_{i,j}^{p+1}-\frac{(k_{pv}+k_e)\Delta y}{2\,\Delta x}T_{i-1,j}^{p+1}-\frac{(k_{pv}+k_e)\Delta y}{2\,\Delta x}T_{i+1,j}^{p+1}-\frac{\Delta x}{\Delta y}\,k_e\,T_{i,j-1}^{p+1}-\frac{\Delta x}{\Delta y}\,k_{pv}\,T_{i,j+1}^{p+1}\right)=T_{i,j}^{p}+\mathbf{L_5}(\Delta x\,\frac{\Delta y}{2}\,Q_{pv})\qquad\textbf{(II.23)}$$

With:

$$\mathbf{L_5}=\frac{2\Delta t}{\Delta x\Delta y\,(\,\rho_{pv}\,c_{pv}+\,\rho_e\,c_e)}$$

- **Type I nodes**

$$\mathbf{L_6}\left(\left(\frac{1}{\mathbf{L_6}}+\frac{(k_t+k_e)\Delta y}{\Delta x}+\frac{\Delta x}{\Delta y}\,k_t+\frac{\Delta x}{\Delta y}\,k_{pv}\right)T_{i,j}^{p+1}-\frac{(k_t+k_e)\Delta y}{2\,\Delta x}T_{i-1,j}^{p+1}-\frac{(k_t+k_e)\Delta y}{2\,\Delta x}T_{i+1,j}^{p+1}-\frac{\Delta x}{\Delta y}\,k_t\,T_{i,j-1}^{p+1}-\frac{\Delta x}{\Delta y}\,k_e\,T_{i,j+1}^{p+1}\right)=T_{i,j}^{p}\qquad\textbf{(II.24)}$$

Where**:**

$$\mathbf{L_6}=\frac{2\Delta t}{\Delta x\Delta y\,(\,\rho_t\,c_t+\,\rho_e\,c_e)}$$

II.4.4. Putting the equations into a matrix form

After having established all the equations for the different nodes, we will write the system of algebraic equations whose resolution allows us to obtain all the temperatures required at the moment $\boldsymbol{t_{p+1}}$. The equations system, consisting of the previously obtained equations, has the following form:

$$\boldsymbol{A\ T^{p+1} = C} \qquad \textbf{(II.25)}$$

With:

- $\boldsymbol{A}$ **:** is a square matrix of dimension N*N;
- $\boldsymbol{T^{p+1}}$**:** is a column vector of dimension N*1 which holds the temperatures of the different nodes at the moment $\boldsymbol{t_{p+1}}$;
- $\boldsymbol{C}$ **:** is a column vector of dimension N*1 which holds straight members (values) of each equation.

The temperatures $\boldsymbol{T^{p+1}}$ are, thus, the solutions of system (II.24), i.e.:

$$\boldsymbol{T^{p+1} = A^{-1}\ C} \qquad \textbf{(II.26)}$$

Chapter III: Results and discussions

III.1. Introduction

About 20% of the solar energy received by the PV cell is converted into electric power, while the rest accumulates as heat. Unfortunately, this additional unwanted heat negatively affects the performance of the PV cell. In order to find the maximum temperature of the cell in Mostaganem city, the thermal model was developed.

However, this model requires calculating certain parameters such as heat exchange coefficients and the generated internal heat. Thus, the objective of this chapter is not only to present the results found, but also to demonstrate how these parameters were calculated.

III.2. Solar radiation

II.2.1. Solar angles

The angles, that define the sun's position in the sky involved in the model, are as follows:

- $\boldsymbol{\beta}$**:** is the tilt angle of the panel in regard to the horizontal plane (assumed to be 20° in this study);
- $\boldsymbol{\gamma}$**:** is the surface azimuth angle (assumed to be 0° in this study);
- $\boldsymbol{\theta_z}$**:** The Zenith angle is the angle between the sun's direction and its projection on a vertical plane. It is calculated with the following formula [Jacobson 05]:

$$\boldsymbol{cos(\theta_Z) = cos(\phi)cos(\delta)cos(\omega) + sin(\phi)\, sin(\delta)} \quad \textbf{(III.1)}$$

Where:

$\boldsymbol{\phi}$**:** is the Latitude;

$\boldsymbol{\delta}$**: declination** is calculated, for the ith day of the year, using Cooper's formula [Duffie 13]:

$$\boldsymbol{\delta = 23.45\, sin(360\, \frac{284+i}{365})} \quad \textbf{(III.2)}$$

$\boldsymbol{\omega}$: **Hour angle**, it represents the angular displacement of the sun east or west due to the rotation of the earth around its axis. It increases by 15° per hour. It is negative in the morning and positive in the afternoon. [Duffie 13].

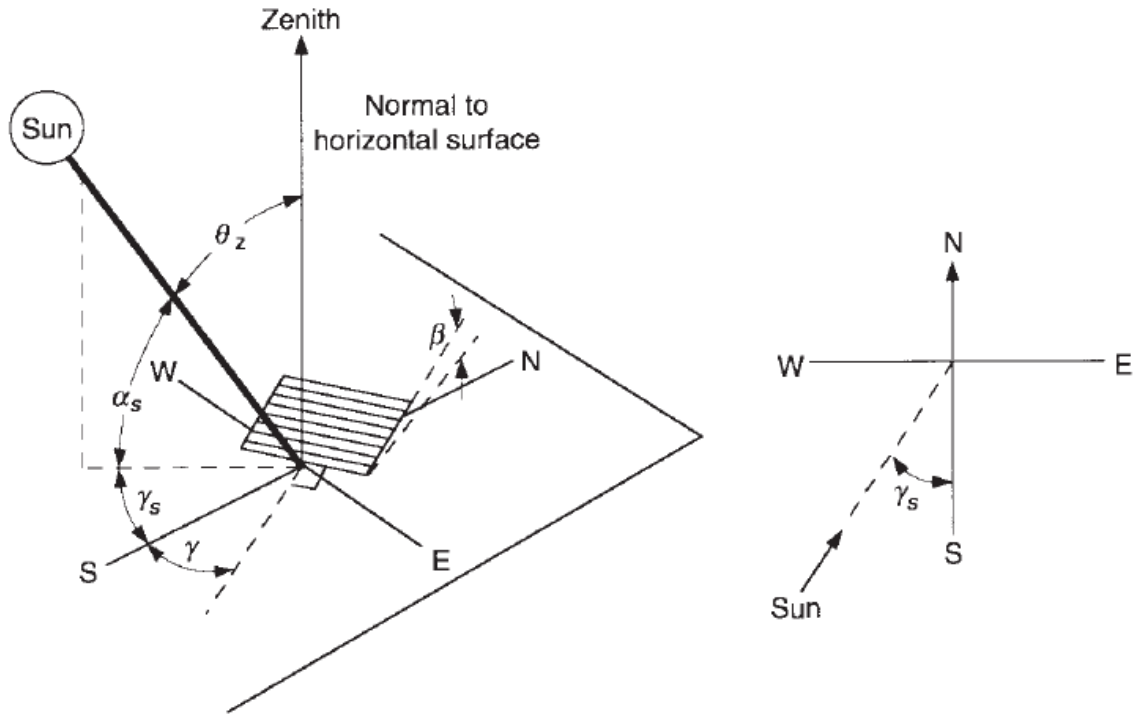

Figure III.1: Solar angles Diagram [Duffie 13].

- $\boldsymbol{\gamma_s}$**:** solar azimuth angle is the angle between the projection of the vertical plane passing through the sun on the horizontal plane and south. It is calculated using the following formula [Duffie 13]:

$$\boldsymbol{\gamma_s = sign(\omega)\ \left|cos^{-1}\left(\frac{cos(\theta_Z)\ sin(\phi) - sin(\delta)}{sin(\theta_Z)\ cos(\phi)}\right)\right|} \qquad \textbf{(III.3)}$$

III.3. The absorbed solar radiation S

The solar radiation incident on the front surface of a photovoltaic panel is not fully absorbed by the PV cells. Part of it is lost by reflection (optical losses), while another part is absorbed through the different layers before reaching the PV cells (e.g. absorption in the front glass). In addition, a PV cell can reflect up to 35% of the irradiation reaching it [Armstrong 10]. The total absorbed solar radiation in the PV cells determines the amount of electrical energy that the PV panel can provide.

The absorbed solar radiation $\boldsymbol{S}$ is calculated using the equation below [Aly1 17]:

$$\boldsymbol{S = \tilde{\alpha}_{PV} * \tau(\theta)_{avg} * G_{POA}} \qquad \textbf{(III.4)}$$

- $\boldsymbol{\tilde{\alpha}_{PV}}$ **:** is the effective absorption of the PV cells (taken as 0.93 in this study);
- $\boldsymbol{G_{POA}}$ **:** is the measured incident POA irradiance;

- $\tau(\theta)_{avg}$**:** is the average transmissivity of the front glass, controlled by the incidence angle of the beam irradiation. (θ_b) [Aly1 17]:

$$\tau(\theta)_{avg} = 0.99\,\tau(\theta_b) \quad \textbf{(III.5)}$$

- θ_b**:** is the angle of incidence of the beam irradiation, it is given by the following relation [Aly1 17, Aly2 17]:

$$\theta_b = \cos^{-1}(\cos\theta_z \cos\beta + \sin\theta_z \sin\beta \cos(\gamma_s - \gamma)) \quad \textbf{(III.6)}$$

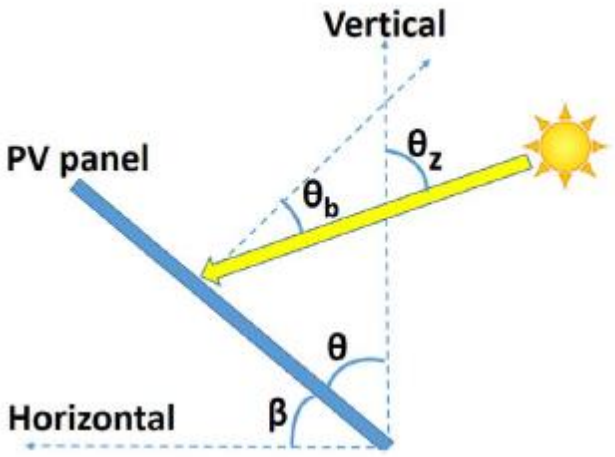

Figure III. 2: Incidence angle for beam solar radiation [Aly1 17].

- $\tau(\theta_b)$: is calculated using the following formula [Aly1 17, Duffie 13]:

$$\tau(\theta_b) = e^{-(KLe/\cos\theta_r)}\left[1 - \frac{1}{2}\frac{\sin^2(\theta_r-\theta_b)}{\sin^2(\theta_r+\theta_b)} + \frac{\tan^2(\theta_r-\theta_b)}{\tan^2(\theta_r+\theta_b)}\right] \quad \textbf{(III.7)}$$

Where:

- ✓ K**:** is the glazing extinction constant (for most PV panels, typical value is 4 m^{-1});
- ✓ Le**:** is the glazing thickness (3 mm considered for the PV panel in this study):
- ✓ θ_r**:** is the refracted angle through the front glass glazing layer obtained using Snell's law [Duffie 13]:

$$\theta_r = \sin^{-1}\left(\frac{n_1}{n_2}\sin\theta_b\right) \quad \textbf{(III.8)}$$

Where:

- n_1**:** is the refractive index of air (n_1= 1).
- n_2**:** is the refractive index of the front glass (n_2= 1.526).

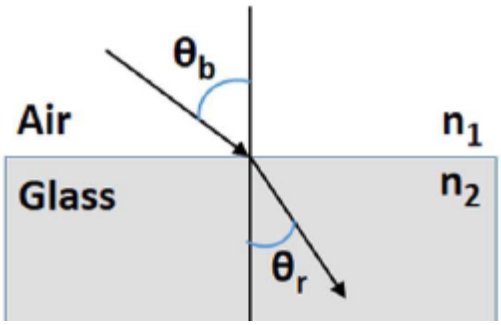

Figure III.3: Refracted angle through the front glass [Aly1 17].

III.4. Generated internal heats

As mentioned in chapter II, heat is only generated inside the glass layer and the PV cell layer.

The heat generated at the glass layer Q_{fg} of the PV panel is given by the following expression [Aly1 17]:

$$\boldsymbol{Q_{fg}=\frac{\alpha_{fg} \times G_{POA} \times A_{PV,panel}}{V_{fg}}} \quad \textbf{(III.9)}$$

- $\boldsymbol{\alpha_{fg}}$**:** is the front glass absorptivity ($\alpha_{fg} = 0.05$).
- $\boldsymbol{A_{PV,panel}}$**:** is the front area of the panel.
- $\boldsymbol{V_{fg}}$**:** is the volume of the front glass.

The energy within the PV cell, not converted into electricity, generates internal heat $\boldsymbol{Q_{pv}}$, can be calculated as follows:

$$\boldsymbol{Q_{pv}=\frac{S \times A_{PV,cells} \times (1-\eta_{PV})}{V_{PV,cells}}} \quad \textbf{(III.10)}$$

- $\boldsymbol{S}$ **:** is the absorbed solar irradiation,
- $\boldsymbol{A_{PV,cells}}$ **:** is the frontal area of the PV cells,
- $\boldsymbol{V_{PV,cells}}$ **:** is the total volume of the PV cells,
- $\boldsymbol{\eta_{PV}}$ **:** is the PV panel's electrical efficiency, which is defined by as [Aly2 17]:

$$\boldsymbol{\eta_{PV} = \eta_{PV,ref}\ (1 - \beta_{ref}(T_{PV,cells} - T_{ref}))} \quad \textbf{(III.11)}$$

- $\boldsymbol{\eta_{PV,T_{ref}}}$ **:** is the electrical efficiency at a reference temperature,
- $\boldsymbol{\beta_{ref}}$ **:** is the temperature coefficient,
- $\boldsymbol{T_{PV,cells}}$ **:** the PV cell temperature,

- T_{ref} **:** the reference temperature.

For our panel ND-220E1 **[**Aly2 17]:

$$\eta_{PV,T_{ref}} = 13.5\% \qquad \beta_{ref} = -0.485\%/°C \quad \text{and} \quad T_{ref}=25°C$$

III.5. Determining the exchange coefficients

III.5.1. Convection exchange coefficients

The convection exchange coefficients h_{con_F/con_R} , indicated in chapter II, are calculated using the formula:

$$h_{con\_F/con\_R} = h_{con\_F\_forced/con\_R\_forced} + h_{con\_F\_fre/con\_R\_free} \quad \textbf{(III.12)}$$

The transfer coefficients by forced and free convection on each side (front and rear faces of the panel) are defined as follows **[**Aly2 17]:

$$h_{forced/free} = \frac{Nu_{forced/free}\ k_{air}}{L_{PV,panel}} \quad \textbf{(III.13)}$$

- k_{air} **:** is the thermal conductivity of air,
- $L_{PV,panel}$ **:** is the characteristic length of the PV panel,
- $Nu_{forced/free}$ **:** is the Nusselt number.

To calculate the Nusselt number of forced convection Nu_{forced}, several formulas can be found in the literature, but the most common is the one proposed by Sparrow [Sparrow 79]:

$$Nu_{forced} = 0.86\,Re^{1/2}Pr^{1/3} \quad \textbf{(III.14)}$$

With:

- ✓ Re **:** is the Reynolds number which has the following expression [Armstrong 10]:

$$Re = \frac{ws * L_{characteristic}}{v} \quad \textbf{(III.15)}$$

ws **:** is the wind speed,

$L_{characteristic}$ **:** is the characteristic length of the PV panel,

v **:** is the kinematic viscosity of air.

- ✓ Pr **:** is the Prandtl number which has the following expression [Armstrong 10]:

$$Pr = \frac{c\mu}{k_{air}} \quad \textbf{(III.16)}$$

Where:

- c **:** is the specific heat of the air,

- μ **:** is the dynamic viscosity of air,
- k_{air} **:** is the thermal conductivity of air.

For natural convection, the Nusselt number Nu_{free} is calculated using the following formula [Aly 18, Aly1 17]:

$$\boldsymbol{Nu_{free}} = \begin{cases} \boldsymbol{0.76Ra^{1/4}} & \boldsymbol{for \quad 10^4 < Ra < 10^7} \\ \boldsymbol{0.15Ra^{1/3}} & \boldsymbol{for \quad 10^7 \leq Ra < 3 * 10^{10}} \end{cases} \qquad \textbf{(III.17)}$$

$\boldsymbol{Ra}$**:** is the Rayleigh number:

$$\boldsymbol{Ra = Gr * Pr} \qquad \textbf{(III.18)}$$

$\boldsymbol{Gr}$**:** is the Grashof number, which is calculated by:

$$\boldsymbol{Gr} = \frac{\boldsymbol{g\beta_{air}(T_{surface} - T_{amb})L^3_{characteristic}}}{\boldsymbol{v^2}} \qquad \textbf{(III.19)}$$

$\boldsymbol{g}$**:** Acceleration of gravity.

$\boldsymbol{\beta_{air}}$**:** air expansion coefficient.

Note that in the relations from (III.13) to (III.19) the physical properties of air are taken at the film temperature $\boldsymbol{T_{film}}$, which is given by the following formula [Armstrong 10, Aly 18, Aly1 17] :

$$\boldsymbol{T_{film}} = \frac{\boldsymbol{T_{sur} - T_{amb}}}{\boldsymbol{2}} \qquad \textbf{(III.20)}$$

III.5.2. Radiation exchange coefficients

The four radiation exchange coefficients listed in the second chapter are calculated using the following formulas [Armstrong 10, Aly1 17]:

$$\boldsymbol{h_{rad\_FS}} = \frac{\boldsymbol{\sigma(T^2_{sur} + T^2_{sky})(T_{sur} + T_{sky})}}{\boldsymbol{\frac{1-0.91}{0.91} + \frac{1}{\frac{1}{2}(1+\cos\beta)}}} \qquad \textbf{(III.21)}$$

$$\boldsymbol{h_{rad\_RS}} = \frac{\boldsymbol{\sigma(T^2_{sur} + T^2_{sky})(T_{sur} + T_{sky})}}{\boldsymbol{\frac{1-0.85}{0.85} + \frac{1}{\frac{1}{2}[1+\cos(\pi-\beta)]}}} \qquad \textbf{(III.22)}$$

$$h_{rad\_FG}=\frac{\sigma(T_{sur}^2+T_{Gr}^2)(T_{sur}+T_{Gr})}{\frac{1-0.91}{0.91}+\frac{1}{\frac{1}{2}(1-\cos\beta)}} \quad \textbf{(III.23)}$$

$$h_{rad\_RG}=\frac{\sigma(T_{sur}^2+T_{Gr}^2)(T_{sur}+T_{Gr})}{\frac{1-0.85}{0.85}+\frac{1}{\frac{1}{2}[1-\cos(\pi-\beta)]}} \quad \textbf{(III.24)}$$

Where:

- ✓ $\boldsymbol{\sigma}$ **:** is the Stefan-Boltzmann constant,
- ✓ $\boldsymbol{T_{sur}}$: is the surface temperature,
- ✓ $\boldsymbol{T_{sky}}$: The sky temperature, it is calculated using the following formula [Aly17]:

$$T_{sky} = 0.0552 * T_{amb}^{1.5} \quad \textbf{(III.25)}$$

- ✓ $\boldsymbol{T_{Gr}}$: the ground temperature, in this work, is assumed to be equal to the ambient temperature.

III.6. Meteorological data of Mostaganem

Due to the health situation in our country, which led to the imposing of a confinement, it was impossible to contact a meteorological station or the national meteorological office to get real meteorological data of Mostaganem. To overcome this problem, it was essential to use a meteorological simulation software.

Thus, we used the software " METEONORM 7.3 ", to estimate the meteorological data of Mostaganem city for the current year. This estimation, which is based on previous data, gives a value every minute.

According to this estimate, the highest temperature will be reached on the 21st of July. Accordingly, meteorological data were chosen to test the obtained thermal model.

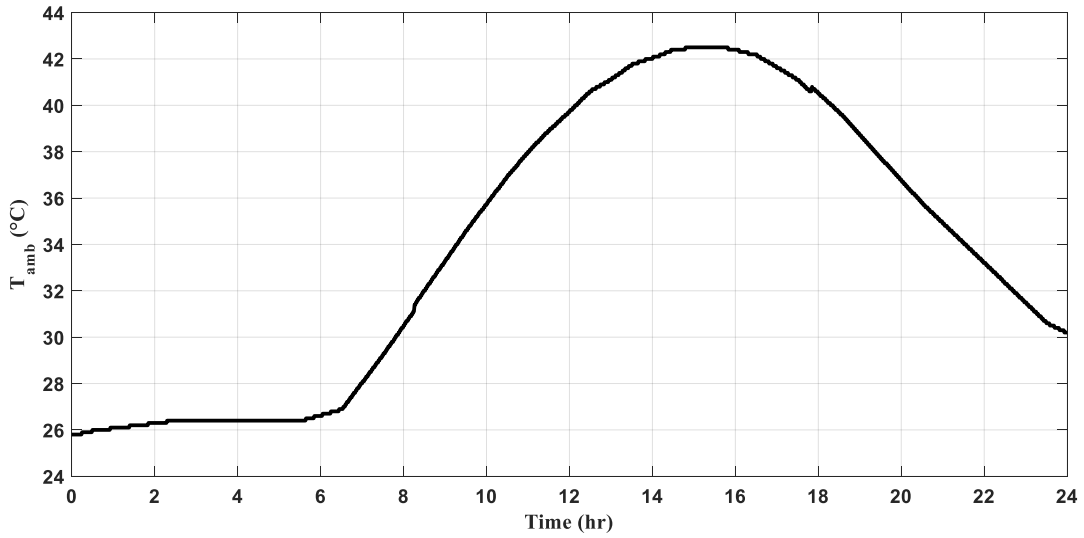

Figure III.4: Estimated ambient temperature for 21/07/2020.

Figure III.4

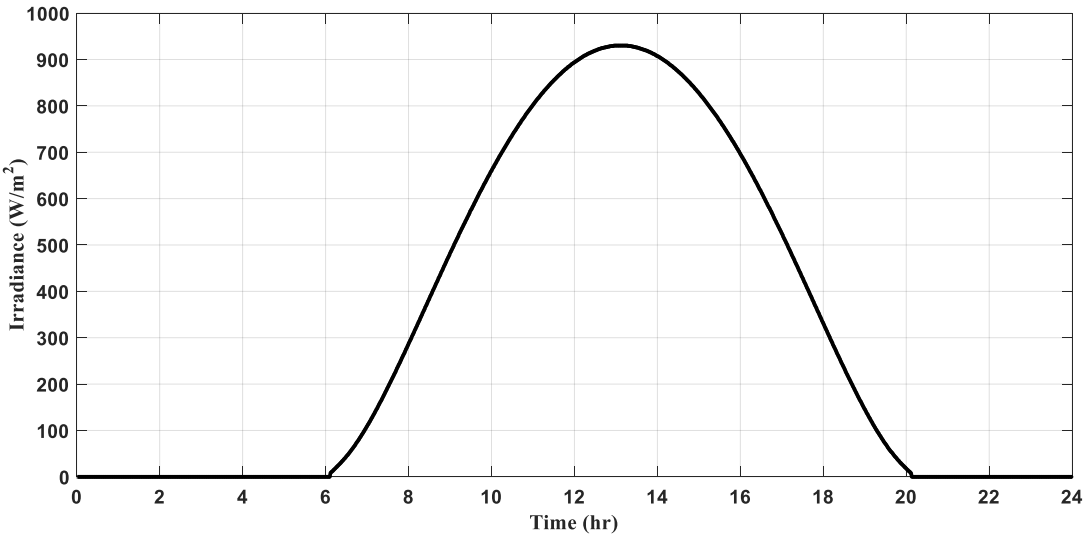

Figure III.5: Estimated POA irradiance for 21/07/2020.

Figures III.4 and III.5 show the estimated ambient temperature and POA irradiance for the day of 21/07/2020. The maximum ambient temperature of this day (42.5°C) is recorded from 14h50min to 15h40min, while the maximum value of the POA irradiance (930 W/m^2) is obtained from 13h00 and 13h30.

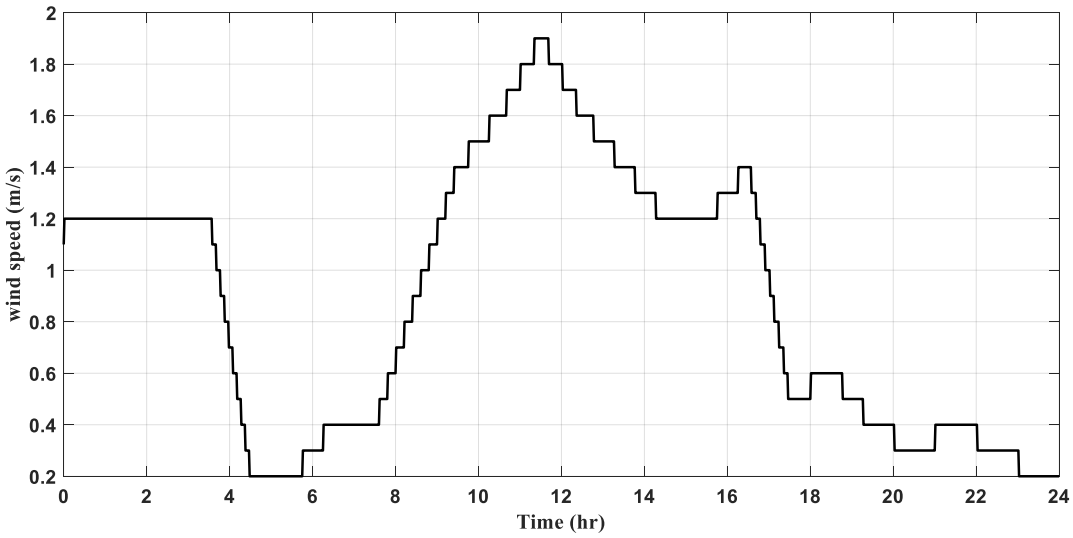

Figure III. 6: Estimated wind speed for 21/07/2020.

Figure III.6 shows the estimated wind speed for the day of 21/07/2020. The maximum wind speed is 1.9 m/s.

III.7. Results and discussions

In order to test the resulting thermal model, we developed a MATLAB script to find the temperature distribution in the PV panel. It should be kept in mind that we are only interested in the temperature variation of the PV cells. Thus, the program visualizes the temperature variation in the PV cells and the variation of the heat exchange coefficients during the selected day. Figure III.7 shows the flowchart of the developed programme.

The program calls up three functions, which do not appear in the flowchart. The functions we created to facilitate the manipulation are:

- A "**data**" function that returns weather data;
- A "**zen**" function that returns the absorbed solar radiation;
- A "**pr_air**" function that receives a temperature and returns the physical properties of air at that temperature.

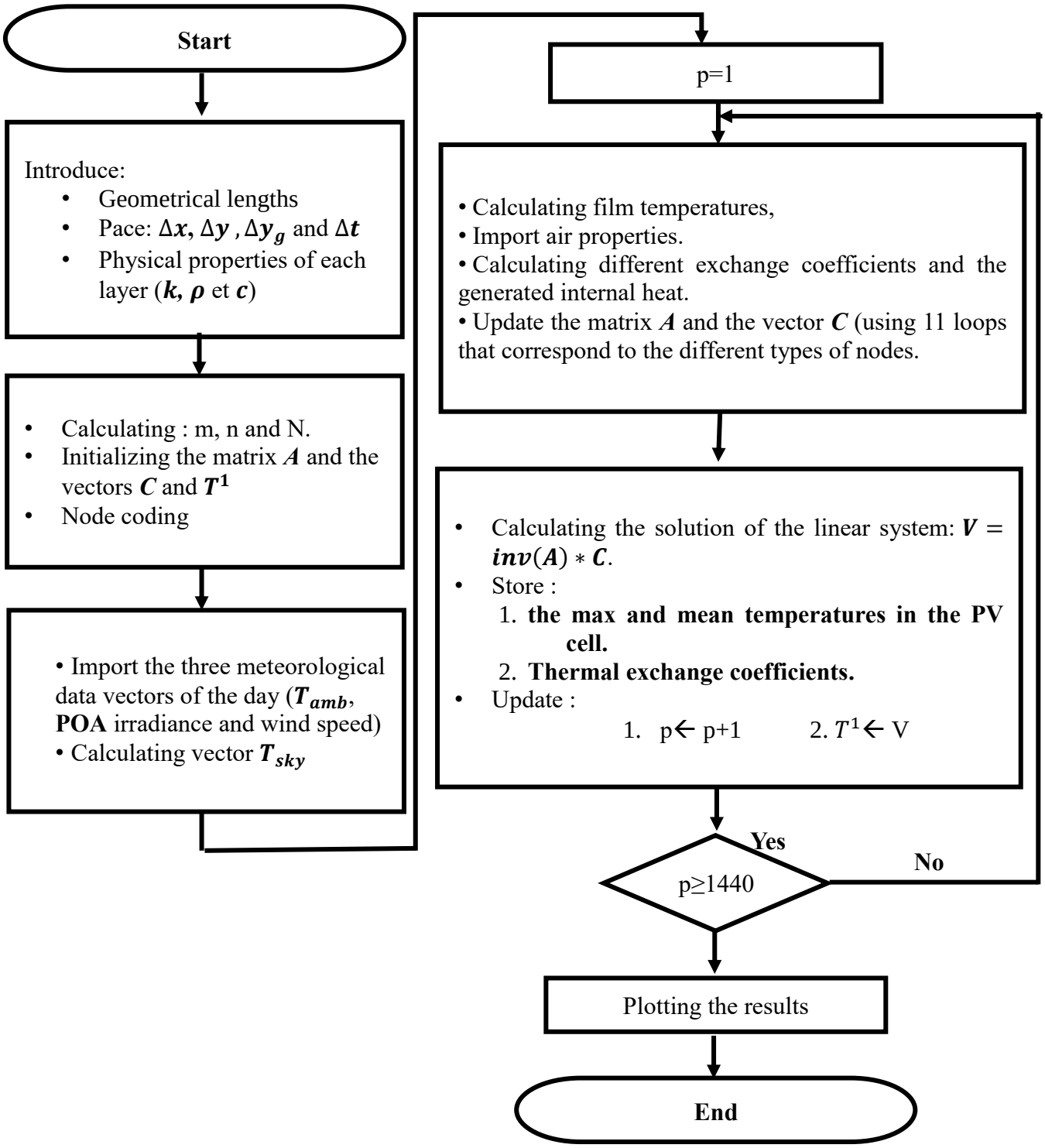

Figure III.7: Program flowchart.

Since the implicit scheme is unconditionally stable, we chose the following steps to test the program: $\Delta x = 8.26\ mm$, $\Delta y = 0.025mm$, $\Delta y_g = 0.5mm$ and $\Delta t = 60s$. This gives a mesh of (101*32) points which is equivalent to 3232 nodes.

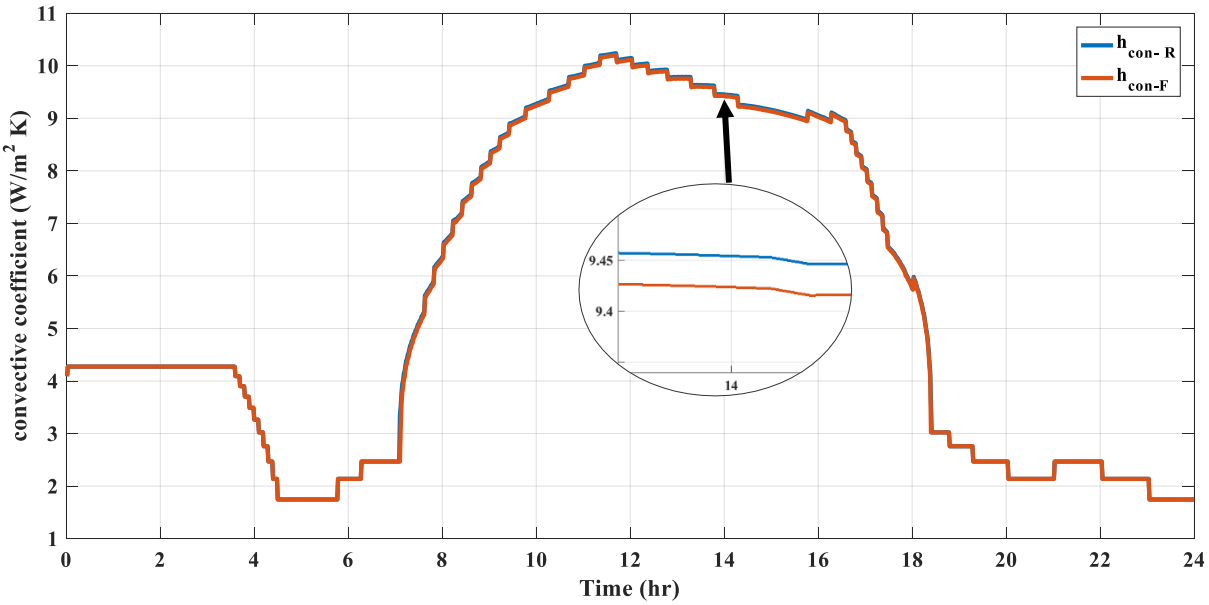

Figure III.8: Variation of the convection coefficients during the day of 21/07/2020.

Figure III.8 shows the variation of the convection exchange coefficients h_{con_F} **and** h_{con_R} during the day. The coefficient on the rear side of the panel is slightly higher than on the opposite side. The highest values are noticed during the period of 8:00 and 16:00.

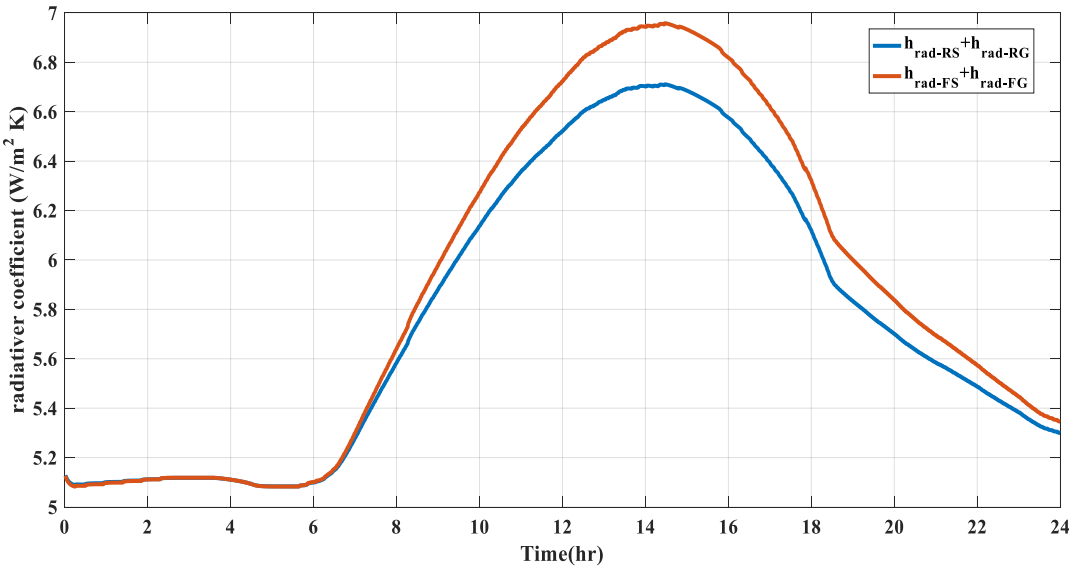

Figure III.9: Variation of the radiation coefficients during the day of 21/07/2020.

Figure III.9 shows the variation in the radiation coefficients during the day of 21/07 on the upper and lower sides of the panel. Here, it is the upper side of the panel that takes over and gives higher values

than those found for the opposite side. This result makes perfect sense since it is the upper side that is most exposed to the sun. The maximum value found for this coefficient (equal to $\boldsymbol{6.96\ W/m^2\ K}$) is comparable to that found by Aly et al [Aly1 17].

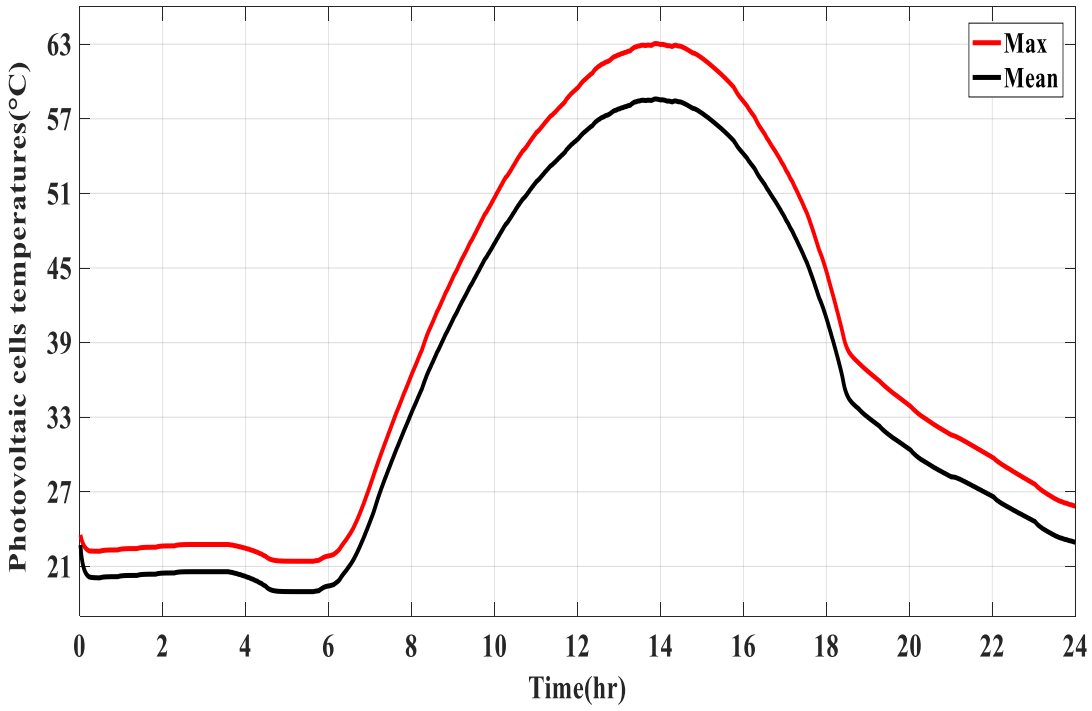

Figure III. 10: Variation of maximum and average PV cell temperatures during the day of 21/07/2020.

The variations in average and maximum temperatures of the photovoltaic cells during the day under study are shown in Figure III.10. The variations are almost linear from midnight to sunrise **(06:00)**.

As the sun rises, the temperatures increase along with the ambient temperature and the solar radiation increases until **13h53min** where the highest values are recorded.

The highest value of the maximum temperatures is **63.05°C** while the highest value of the average temperatures is **58.59°C**. The maximum difference between the values of the maximum and average temperatures is **4.46°C.**

CONCLUSION

Photovoltaic energy is becoming increasingly important worldwide. Indeed, these energies are not only clean, but also sustainable. That is why Algeria has made significant investments to produce 18% of electricity for national consumption from photovoltaic energy [Era 20]. In order to achieve these objectives, it is essential to make optimal use of solar panels.

Among the factors that affect the efficiency of PV panels is the operating temperature of the PV cells. The objective of this study was to develop a program to estimate the temperature of the PV cells depending on the daily change in climatic conditions.

By the completion of this study, we were able to achieve the following:

- ✓ Detail the thermal model proposed by Aly et al [Aly2 17], taking into account the meteorological variables: ambient temperature, radiation and wind speed.
- ✓ Estimate the meteorological data of Mostaganem city for the current year using the "Meteonorm 7.3" software.
- ✓ Create a program that allows us to visualize the daily variation of:
    - o convection exchange coefficients,
    - o radiation exchange coefficients,
    - o average and maximum photovoltaic cell temperatures.

The obtained results are comparable to those found in the literature and are satisfying. However, the program is very computationally costly. In fact, it took an "intel Core i3-M370 2.40 GHz processor with 4 GB of RAM" about 3 hours and 54 minutes to execute this program for 3232 Nodes and a time step of 60 seconds.

The perspectives offered by this study are as follows:

- ✓ simulate the effect of meteorological variables on the performance of solar panels;
- ✓ replace the direct method of solving linear systems with iterative methods, in order to reduce calculation time.

BIBLIOGRAPHY

[Alive 20] https://www.alivegreenpower.com/how-do-photovoltaic-cells-work, Last access: June 2020.

[Aly 18] Shahzada Pamir Aly, Said Ahzi, Nicolas Barth, Amir Abdallah, « Using energy balance method to study the thermal behavior of PV panels under time-varying field conditions », Energy Conversion and Management 175 (2018) 246–262, https://doi.org/10.1016/j.enconman.2018.09.007.

[Aly1 17] Shahzada Pamir Aly, Said Ahzi , Nicolas Barth, BenjaminW.Figgis, Two-dimensional finite difference-based model for coupled irradiation and heat transfer in photovoltaic modules, Solar Energy Materials and Solar Cells (2017), http://dx.doi.org/10.1016/j.solmat.2017.06.055.

[Aly2 17] Shahzada Pamir Aly, Nicolas Barth, BenjaminW.Figgis, Said Ahzi, A fully transient novel thermal model for in-field photovoltaic modules using developed explicit and implicit finite difference schemes, Journal of Computational Science https://doi.org/10.1016/j.jocs.2017.12.013.

[Armstrong 10] S. Armstrong, W.G. Hurley . « A thermal model for photovoltaic panels under varying atmospheric conditions », Applied Thermal Engineering 30 (2010) 1488e1495, doi:10.1016/j.applthermaleng.2010.03.012.

[Azzi 11] Abbès AZZI « méthodes numériques appliquées aux calculs des écoulements et du transfert de chaleur », Faculté de Génie-Mécanique, USTO, www.abbesazzi.com , Juin 2011.

[Banaceur 19] Banaceur fatima zohra et Baazzi aicha. « Etude démonstrative des différents défauts des systèmes photovoltaïques installés au sein de l'URERMS Adrar », Mémoire De Master En Electrotechnique Option:Commande Electrique Département Des Sciences et Technologie Faculté Des Sciences et de Technologies Université Ahmed Draia Adrar, 2019.

[Benbrik 18] A. Benbrik ,« Support de cours Transferts de Chaleur Tome 1 : Conduction », département de transport et équipements des hydrocarbures, faculté des hydrocarbures et de la chimie université M'hamed Bougara(boumerdès), 2018.

[Çengel 03] Y. A. Çengel. *Heat transfer: A Practical Approach*. 2nd edition, McGraw-Hill, 2003.

[Clean 20] https://www.cleanenergyreviews.info/blog/pv-panel-technology Last access: June 2020.

[Čotar 12] Andrej Cotar, et al. "Photovoltaic Systems, Commissioning party: IRENA- Istrian Regional Energy Agency"; January 2012. http://www.irena-istra.hr/uploads/media/Photovoltaic_systems.pdf

[Dubey 13] Swapnil Dubey, Jatin Narotam Sarvaiya, Bharath Seshadri, « Temperature Dependent Photovoltaic (PV) Efficiency and Its Effect on PV Production in the World A Review » Energy Procedia 33 (2013) 311 – 321 doi: 10.1016/j.egypro.2013.05.072.

[Duffie 13] J.A. Duffie, W.A. Beckman, Solar Engineering of Thermal Processes, 4th ed., Wiley, New Jersey, 2013.

[Energy 20] https://news.energysage.com/what-are-the-most-efficient-solar-panels-on-the-market/ Last access: June 2020.

[Era 20] https://era.dz/salon/fr/content/programme-national-des-%C3%A9nergies-nouvelles-et-renouvelables Last access: June 2020

[Gov 20] https://www.energy.gov.dz/?rubrique=energies-nouvelles-renouvelables-et-maitrise-de-lrenergie, Last access: June 2020.

[Giovannini 12] A. Giovannini et B. Bédat « Transfert de chaleur » édition Cépadus, septembre 2012.

[India 20] https://www.indiamart.com/proddetail/pv-direct-solar-system-20730124548.html Last access: June 2020.

[Irwanto 14] Irwanto, Muhammad & Yusoff, Mohd & Ibrahim, Safwati & Wai Zhe, Leow & Nair, Gomesh. (2014). Analysis simulation of the photovoltaic output performance. Proceedings of the 2014 IEEE 8th International Power Engineering and Optimization Conference, PEOCO 2014. 477-481. 10.1109/PEOCO.2014.6814476.

[Jacobson 05] Jacobson, Mark Z. . Fundamentals of Atmospheric Modeling (2nd ed.). Cambridge University Press. p. 317. ISBN 0521548659., 2005.

[Necati 17] M. Necati Özis¸ik , Helcio R.B. Orlande , Marcelo José Colaço Renato Machado Cotta « Finite Difference Methods in Heat Transfer- Second Edition », Taylor & Francis Group, 2017.

[Seia 20] https://www.seia.org/initiatives/photovoltaics Last access: June 2020.

[Siddiqui 12] M.U. Siddiqui, A.F.M. Arif, L. Kelley, S. Dubowsky, Three-dimensional thermal modeling of a photovoltaic module under varying conditions, Sol. Energy 86 (2012) 2620–2631, http://dx.doi.org/10.1016/j.solener.2012.05.034.

[Silva 07] Eric Goncalvès da Silva. « Méthodes et Analyse Numériques ». Engineering school. Institut Polytechniquede Grenoble, 2007, pp.99. cel-00556967.

[Solarm 20] https://solarmagazine.com/solar-panels/ Last access: June 2020.

[Solarp 20] https://solarpanelsvenue.com/types-of-solar-panels-most-used-pv-solar-panels/ Last access: June 2020.

[Sparrow 79] E.M. Sparrow, Effect of finite width on heat transfer and fluid flow about an inclined rectangular plate, J. Heat. Transf. 101 (1979) 199.

[Spirit 20] https://www.spiritenergy.co.uk/kb-solar-panel-efficiency Last access: June 2020.

[Sumathi 15] S. Sumathi, L. Ashok Kumar and P. Surekha, Solar PV and Wind Energy Conversion Systems An Introduction to Theory, Modeling with MATLAB/SIMULINK, and the Role of Soft Computing Techniques, Springer International Publishing, April 2015.

[Zeman 10] Zeman, M. (n.d.). Introduction to photovoltaic solar energy, delft university of technology. http://aerostudents.com/files/solarCells/solarCellsTheoryFullVersion.pdf. Retrieved 15 September 2010.

[Zondag 02] H.A. Zondag, D.W. de Vries, W.G.J. van Helden, R.J.C. van Zolingen, A.A. van Steenhoven, The thermal and electrical yield of a PV-thermal collector, Sol. Energy 72 (2002) 113–128, http://dx.doi.org/10.1016/S0038-092X(01)00094-9.

[Zhao 99] Zhao J, Wang A, Campbell P, Green. MA. A 19.8% efficient honeycomb multicrystalline silicon solar cell with improved light trapping. IEEE Transactions on Electron Devices 1999;46:1978–83.